Characterization, electrical and optical properties of PVA/MnO₂ nanocomposite materials

B. M. Alotaibi[a], H. A. Al-Yousef[a], A. Atta[b,*], F.Taher[c,d]
aPhysics Department, College of Science, Princess Nourah bint Abdulrahman University, Riyadh, Saudi Arabia
bPhysics Department, College of Science, Jouf University, P.O. Box: 2014, Sakaka, Saudi Arabia
cChemistry Department, Faculty of Science, Al-Azhar University (Girls), Nasr city, Cairo, Egypt
dAl-Azhar Technology Incubator (ATI), Nasr city, Cairo, Egypt

In this research, various concentrations of manganese dioxide (MnO_2) is composed by polyvinyl alcohol (PVA) to forming PVA/MnO_2 films. The XRD and SEM are respectively demonstrated the structure and morphological characteristics of the films. The XRD results show that the PVA/MnO_2 films is fabricated successfully. The SEM results demonstrate that MnO_2 is dispersed evenly along the PVA polymeric chains. The conductivity, impedance and energy density were measured via an LCR bridge with frequency 10^2 to 10^6 Hz. There is an increase in dielectric from 64 for PVA to 95 for PVA/0.06MnO_2 at 10^5 Hz, and also the conductivity increases from 3.61×10^{-3} S/cm for PVA to 5.33×10^{-3} S/cm for PVA/0.06MnO_2. The optical characteristics of PVA and PVA/MnO_2 films were recorded by UV/Vis spectroscopy. The band gap reduced from 5.01 eV for PVA to 4.85, 4.71, 4.59 eV respectively for PVA/0.02MnO_2, PVA/0.04MnO_2, and PVA/0.06MnO_2. And the Urbach tail is modified from 1.72 eV for PVA to 3.12, 3.453, and 3.66 eV respectively. The results of the present work open the possibility for applied in different devices as energy storage systems and optoelectronics.

1. Introduction

The incorporating of nano-additives into polymeric matrix, are able to create composite polymeric films with very specialized applications. [1,2]. These composites have found use in a number of different technological applications, including super-capacitors and optoelectronics [3]. Composite materials with distinct optical and electrical properties are applied as substances for different devices [4]. As a result of combining the polymer's machinability, endurance, and ductility, composite films have significant practical applications [5, 6].

Metal oxide has potential uses in optoelectronics devices as well as electrical efficiency [7]. Due to its storage properties, MnO_2 has captured the attention of nanostructured materials researcher [8]. Many industries have taken an interest in using of MnO_2 in sensors, battery, and optoelectronics [9]. The impact of adding inorganic nanoparticles to matrix materials on the conductance and optoelectronics properties of polymeric films has been the subject of several researches [10]. In contrast side, the introduction of MnO2 induced of structural and chemical modification in the composite properties [11]. Dispersed nanoscale MnO_2 is significantly more effective than micro scale MnO_2 [12]. More susceptibility to deterioration with dispersal homogeneity is also provided by MnO_2 [13]. The development of electrical pathways through composite films and electron transit through electrical pathways are the two features of the conductivity process that are maximized [14,15].

With the use of various preparation techniques, PVA synthetic polymer might well be handled easily and molded into films [16]. Extensive research has been conducted on the chosen PVA polymer as a great host material [17]. Despite this, PVA hydrophilic nature, chemical durability, and isolating dielectric qualities make it a common material in circuits for electronics [18, 19]. PVA can be exploited as an excellent-bonded material in with the filler to forming the polymer composites [20]. This work is aimed to improve the PVA/ MnO_2 optical and electrical behavior for applied these films in different devices as energy storage and optoelectronics.

2. Experimental work

PVA/MnO_2 is prepared utilizing solution cast preparing procedure [21, 22], with different content of MnO_2 (0.02 to 0.06) dispersed in PVA polymeric films. The PVA/MnO_2 composite films, in thickness of 0.4 mm, were cast in petri dishes, and given a 24-hour drying period in a 40 °C oven. The films are divided into 1.6 x1.6 cm pieces for characterization examination. To ascertain the structural, XRD (Shimadzu-6000) was used. In order to analyze the morphology, SEM (JEOL; Japan) is used. A programmed LCR meter (3531Z, Hioki, Japan) is used to measure the dielectric properties at frequencies between 10^2 and 10^6 Hz. The UV/VIS (JascoV-670) is used to determine the UV-vis absorption of PVA/MnO_2 films in wavelength of 220 to 1050 nm.

3. Results and discussion

Figure 1 indicate the XRD patterns of PVA and MnO_2/PVA films. The picture reveals only one peak for PVA about 2θ=19.8º, showing that PVA has a semi-crystalline structural [22]. The MnO_2 is verified by shifting of PVA diffraction peak, as seen in Figure 1 [23]. This is owing to the high number of hydrogen bonds that exist between PVA chains and MnO_2. The crystallite size of MnO_2 was given using Debye-Scherer D=$(0.9*\lambda)/(\beta\cos\theta)$ [24]. The calculated crystallite size D of MnO_2 is in the range of 22.6 nm.
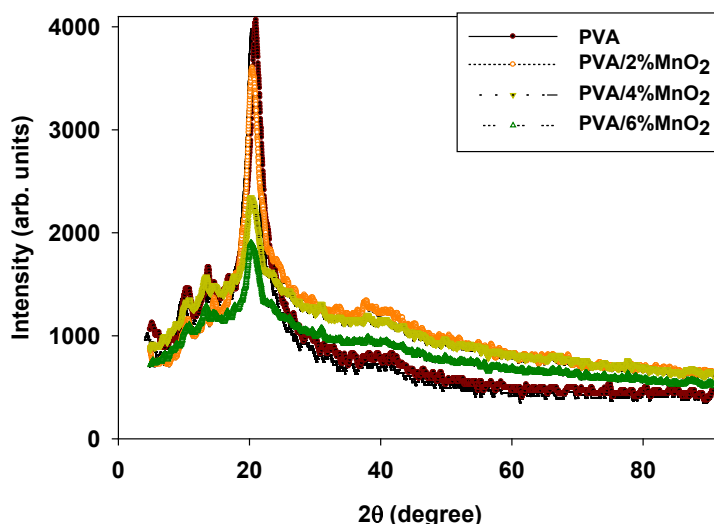
Fig. 1. XRD of PVA, PVA/2%MnO₂, PVA/4%MnO₂, and PVA/6%MnO₂.

SEM images of PVA, PVA/2%MnO_2, PVA4%MnO_2, and PVA/6%MnO_2 films are shown in Figs. 2(a-d). The morphologies of the pure PVA film are depicted in Fig. 2a, which reveals that the surface is smooth and homogeneous [25]. Furthermore, as seen in in Figs. 2(b-d), the SEM images of PVA/MnO_2 upon incorporation of MnO_2 indicates the production of white spots with the creation of certain tiny aggregates, indicating the development of MnO_2 in the PVA matrix. The

discrepancy in surface morphologies detected upon introduction of MnO_2 can be attributed to the effective dispersing of MnO_2 in the PVA [26]. The homogenous incorporation of MnO_2 in PVA matrix is enhanced by raising MnO_2 content (as shown in Fig.2b, c and d).
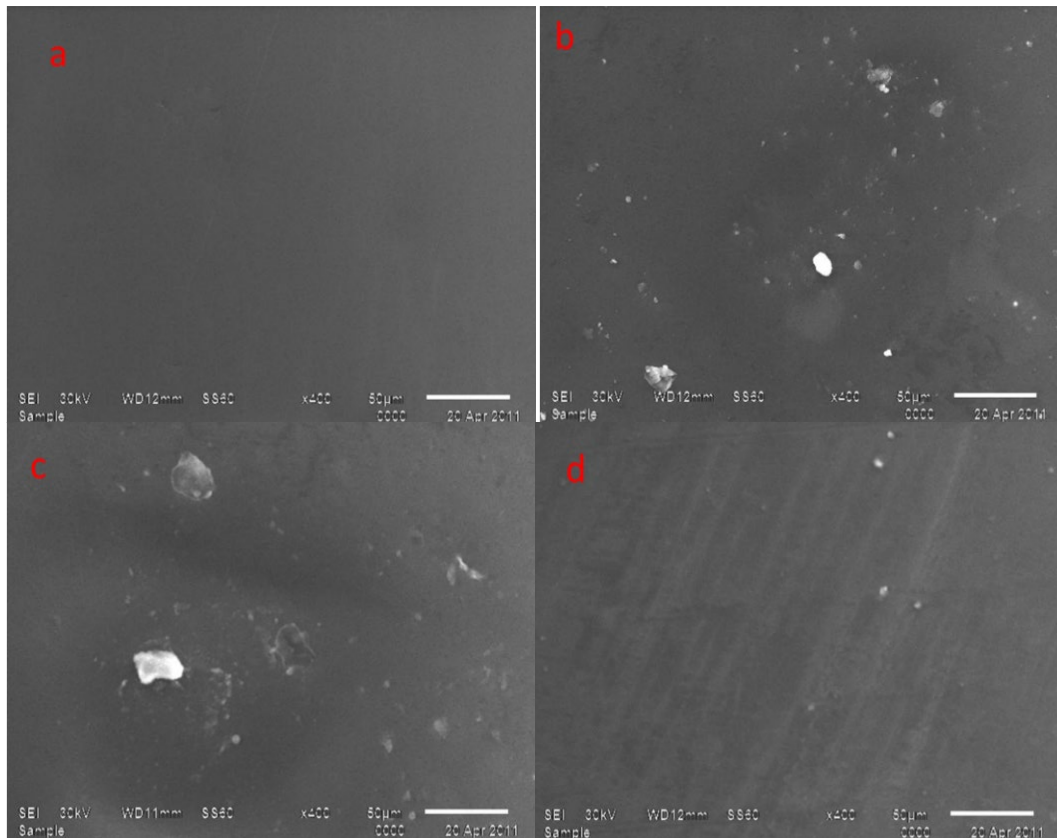
Fig. 2. SEM of (a) PVA, (b) PVA/2%MnO₂,(c) PVA/4%MnO₂ and(d) PVA/6%MnO₂.

The dielectric constant $\varepsilon^{`}$, is estimated from by [27].

$$\varepsilon^{`} = \frac{C \cdot d}{\varepsilon_o \cdot A} \tag{1}$$

where, C corresponds to capacitance, A corresponds to area, ε_o corresponds to permittivity 0.89×10^{-11} F/m, and d is the thickness. The $\varepsilon^{`}$ with frequency for PVA, PVA/0.02MnO₂, PVA/0.04MnO₂, and PVA/0.06MnO₂ are plotted in Fig. 3.
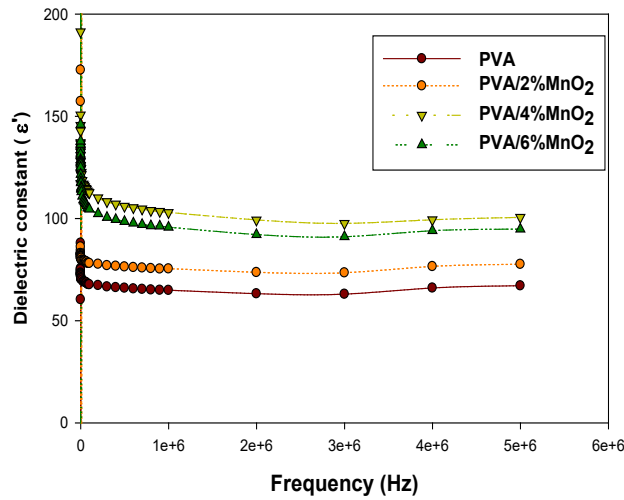
Fig. 3. ε' with frequency of PVA and PVA/MnO$_2$.

The ε' is affected by the frequency due to the motion of carriers within the substance. Since the charge contributions is crucial in the polarizability process, increasing the supplied frequency causes a shift in ε' [28]. In Table 1, we see that the ε' enhanced from 64 for pure PVA to 75 for PVA/0.02MnO$_2$ and 102 for PVA/0.04MnO$_2$ at a frequency of 10^5 Hz. The generated charge carrier quantities cause the rise in ε' value caused by MnO$_2$ concentrations.

The imaginary ε'', is estimated by the loss tangent (tan δ) by formula [29].

$$\varepsilon'' = \varepsilon' \tan\delta \qquad (2)$$

Figure 4 shows the correlated ε'' with frequency for pure PVA and PVA/MnO$_2$. The ε'' modified by frequency for all films; this really is owing to the charge transport [30]. The ε'' with frequency is changed, due to the difference in electronic oscillation [31]. At 10^5 Hz, ε'' changed from 2.5 for PVA to 2.1 for PVA/0.02MnO$_2$ and 5.7 for PVA/0.06MnO$_2$. The enhanced in ε'' is because the connections between PVA and MnO$_2$. The variation in dielectric permittivity readings of PVA/MnO$_2$ films over frequency is due to the alteration in polarization [32]. The enhanced of permittivity which caused by MnO$_2$ are due to the dipolar relaxing characteristic feature that is more beneficial in the lower frequencies zone [33]. The dispersal of MnO$_2$ in the PVA polymeric chains is caused the creation of defective states in PVA.
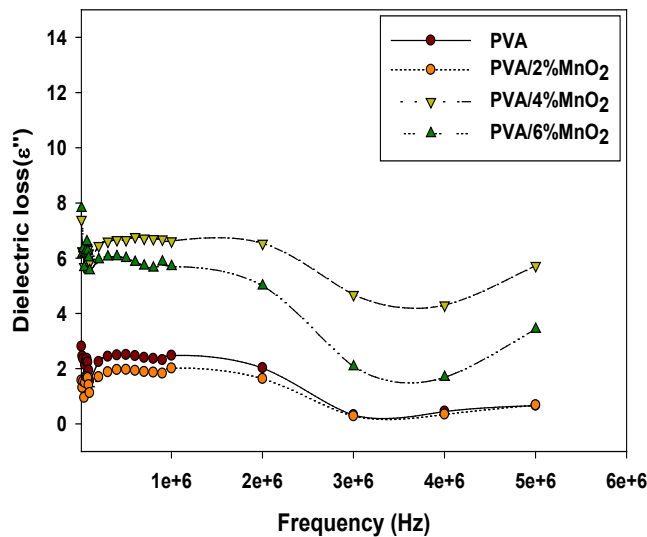
Fig .4. ε'' with frequency of PVA and PVA/MnO$_2$.

The electrical complex modulus M, is given by [34].

$$M = \frac{1}{\varepsilon' + i\varepsilon''} = M' + i\,M'' \tag{3}$$

where, M'' and M' are imaginary and real modulus. The real $M' = \frac{\varepsilon'}{\varepsilon'^2 + \varepsilon''^2}$, whereas imaginary $M'' = \frac{\varepsilon''}{\varepsilon'^2 + \varepsilon''^2}$. The variations of M' by frequency for PVA, PVA/0.02MnO$_2$, PVA/0.04MnO$_2$, and PVA/0.06MnO$_2$ are seen in Fig. 5. The M' is modified with supplied frequency of whole samples, that support the polarization electrode contribute insignificantly to the materials [35]. It is obvious the M' of the films change with increase of frequencies and become constant at high frequency, this is because of free charges and conductance impedance. The M' decreases from 0.0154 for pure PVA to 0.0133 for PVA/0.02MnO$_2$ and 0.0104 for PVA/0.06 MnO$_2$. This is because MnO$_2$ inclusion rises the conductivity and diminish composite film relaxing.
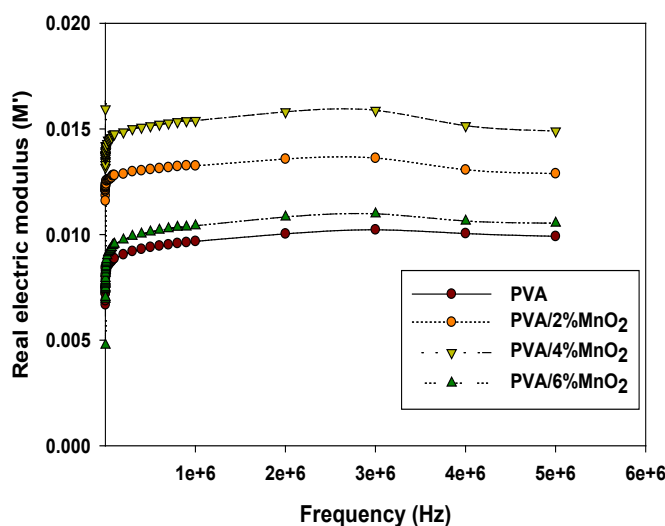
Fig. 5. M' versus frequency of PVA and PVA/MnO$_2$.

The relation of M" by frequency for PVA, PVA/0.02MnO$_2$, PVA/0.04MnO$_2$, and PVA/0.06MnO$_2$ samples is plotted in Fig. 6. Increased permittivity, in lower frequency, is a result of the free dipolar functional [36]. The contributions of these dipolar groups tend to decrease in higher frequency because of the increased difficulty in reorienting such groups. At 10^5 Hz, the M" decreased from 4.9×10^{-4} for PVA to 3.5×10^{-4} for PVA/0.02MnO$_2$. This decrease is because the inclusion of MnO$_2$ [37]. The enhancement of density and charge localized carriers is increases the conductivity the electrical modulus falls. Figure 6 depicts the relaxing peak of the M". With raising the content of MnO$_2$, the strength of the relaxing peak is diminished. The chains relaxation time τ_r is calculated using the relationship [38,39].

$$\tau_r = \frac{1}{2\pi f_p} \tag{4}$$

f_p is the supplied frequency at the relaxing peak. The relaxation time falls from 1.99×10^{-5} sec for pure PVA to 1.77×10^{-5} sec for PVA/0.02MnO$_2$, changed to 3.18×10^{-5} sec for PVA/0.04/MnO$_2$ and reached to 1.87×10^{-5} sec for PVA/0.06MnO$_2$. This is due to the dispersing of MnO$_2$ within PVA [40,41]. The decrease in relaxation time τ_r caused by MnO$_2$ is owing to their flexibility and higher conductivities. These findings suggest that PVA/MnO$_2$ composites films might be attractive options for high-speed optoelectronics.
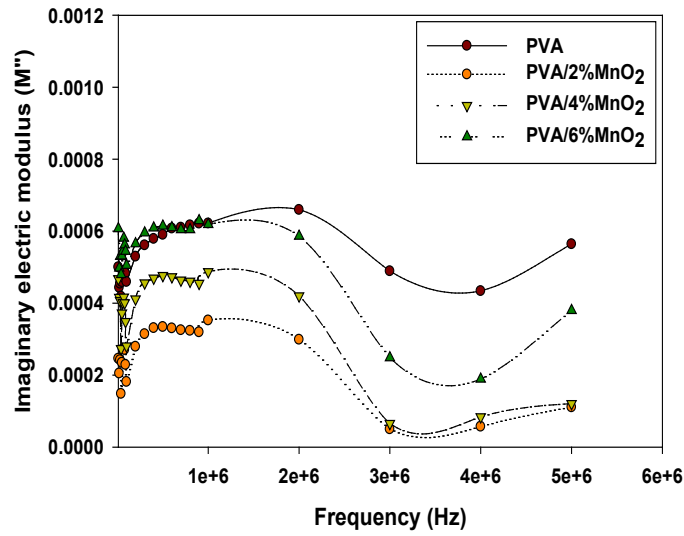
Fig. 6. M'' versus frequency of PVA and PVA/MnO$_2$.

The energy density (U) is calculated by [42], where E is the external electric field.

$$U = \frac{1}{2}\, \varepsilon' \varepsilon_O\, E^2 \tag{5}$$

The U is plotted with frequency for PVA, PVA/0.02MnO$_2$, PVA/0.04MnO$_2$, and PVA/0.06MnO$_2$ samples, as in Fig. 7. The U value of composite PVA/MnO$_2$ is higher if compared to PVA. At 10^5 Hz the U value is increased from $2.87*10^{-10}$ J/m^3 for PVA to $3.34*10^{-10}$ J/m^3 for PVA/2%MnO$_2$ and to $4.55*10^{-10}$ J/m^3 for PVA/4%MnO$_2$.
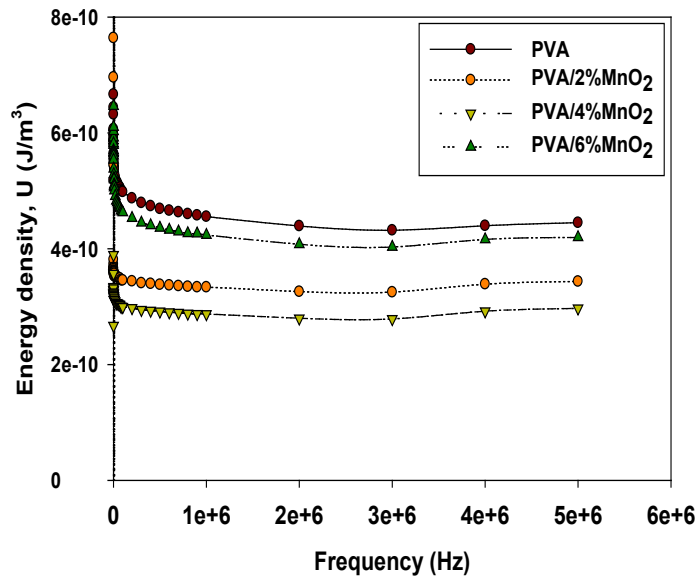
Fig. 7. U versus frequency of PVA and PVA/MnO$_2$ samples.

Table 1. The values of $\varepsilon^`$, $\varepsilon^{``}$, m', m'', σ_{ac} and U for PVA and , PVA/MnO$_2$ samples.

	$\varepsilon^`$	$\varepsilon^{``}$	M'	M''	$\sigma_{ac (S/cm)}$	$U(J/m^3)$
PVA	64	2.5	0.0154	0.00049	$3.61*10^{-3}$	$2.87*10^{-10}$
PVA/2%MnO$_2$	75	2.1	0.0133	0.00035	$4.19*10^{-3}$	$3.34*10^{-10}$
PVA/4%MnO$_2$	102	6.6	0.0096	0.00063	$5.73*10^{-3}$	$4.55*10^{-10}$
PVA/6%MnO$_2$	95	5.7	0.0104	0.00062	$5.33*10^{-3}$	$4.23*10^{-10}$

The relationship of electrical conductivities σ_{ac} and frequency exponent (S) is given by [43]:

$$\sigma_{ac} = A\omega^S \tag{6}$$

S denotes the frequency exponent, where ω is the angular frequency. Figure 8 displays the frequency-dependent σ_{ac} of PVA and PVA/MnO$_2$ films. The σ_{ac} is improves with increasing frequency, for all films, possibly because of the applied electric field [44]. According to Table 1, at an applied frequency of 1MHz, the σ_{ac} is raised from $3.61*10^{-3}$ S/cm for pure PVA to $4.19*10^{-3}$ S/cm for PVA/2%MnO$_2$ and to $5.33*10^{-3}$ S/cm for PVA/6%MnO$_2$. This is because when MnO$_2$ is incorporated into PVA, the localized states are broken up, bridging the gap and allowing the charge carrier to be transported [45,46].
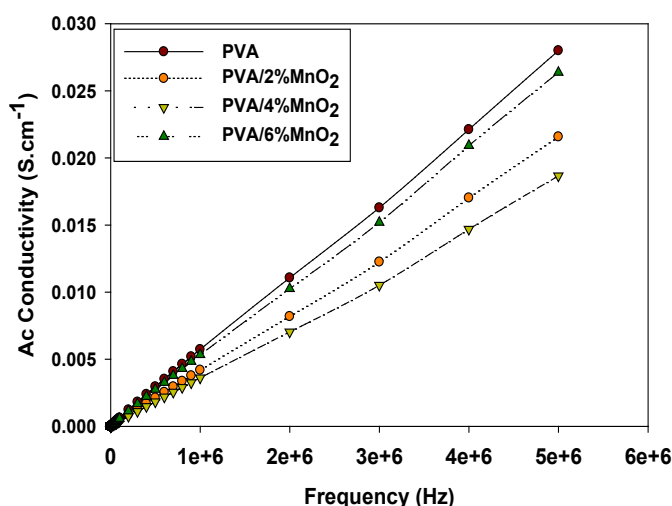
Fig. 8. σ_{ac} with frequency of PVA, PVA/2%MnO$_2$, PVA/4%MnO$_2$, and PVA/6%MnO$_2$.

The value of S varied of 0.989 for PVA to 0.988 for PVA/0.02 MnO$_2$, 0.964 for PVA/0.04 MnO$_2$, and 0.965 for PVA/0.06MnO$_2$. The reason for the shift in S is due to the induced defect density in MnO$_2$. The following relation [47] is given to estimate the height barrier W$_M$,

$$W_m = \frac{6K_B T}{1-S} \tag{7}$$

k$_B$ is Boltzmann constant in eV, T is temperature, and W$_m$ is the needed energy to move an electron indefinitely. As illustrated in Fig. 9, the calculated W_m value varied with growing MnO$_2$ content, ranging from 14.2 eV for PVA to 13.1 eV for PVA/0.02MnO$_2$, 4.35 for PVA/0.04 MnO$_2$, and 4.48 for PVA/0.06MnO$_2$.
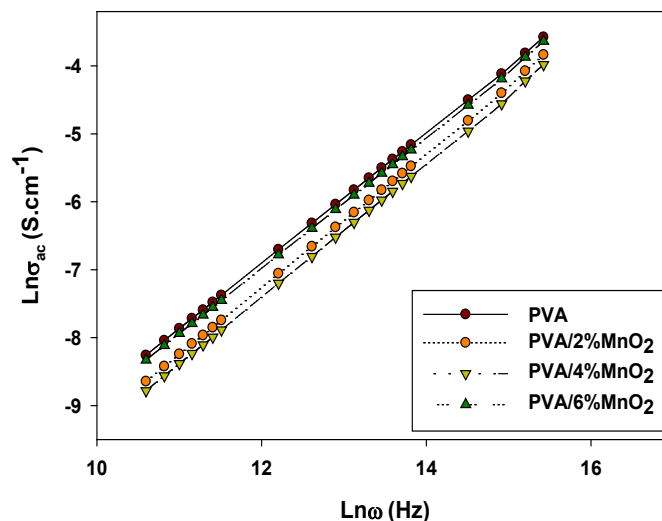
Fig. 9. Ln (σ_{ac}) with Ln (ω) of PVA and PVA/MnO$_2$.

Figure 10 displays the absorption for both PVA and PVA/MnO$_2$. In PVA/MnO$_2$ composites, the shift of absorbance peak over PVA confirms the presence of both PVA and MnO$_2$, with an increase in absorption intensity by MnO$_2$ concentrations. The Beer-Lambert expression used to determine the absorption coefficient (α) by [48]:

$$\alpha = \frac{2.303\ A}{d} \tag{8}$$

Figure 11 shows the correlation between coefficients (α) and hv for PVA and MnO$_2$. It is demonstrated that the introduction of MnO$_2$ causes flaws in the composite, leads to enhancing of absorption coefficient of PVA. As shown in Table 2, the absorption edge (E$_e$) is calculated by extrapolating linear segments versus hv to reach zero absorption. The E$_e$ for PVA film is determined to be 3.93 eV, varying to 3.75 eV for PVA/0.02MnO$_2$, 3.31 eV for PVA/0.04MnO$_2$, and 2.76 eV for PVA/0.06MnO$_2$. This shift to lower photon energy demonstrates a narrowing of the band gap (E$_g$) in PVA/MnO$_2$ composites.
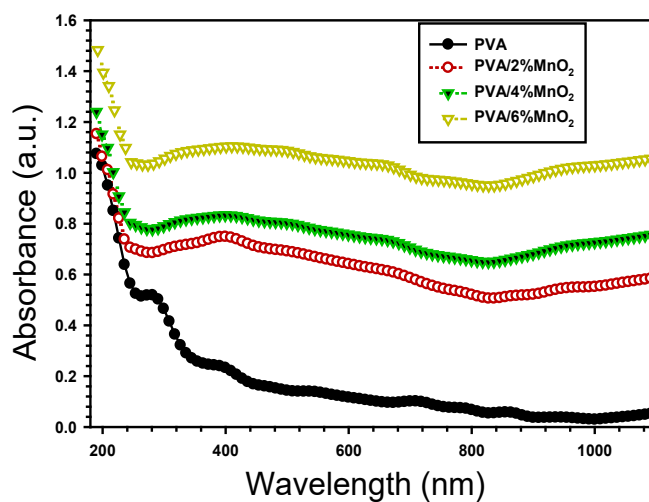
Fig. 10 *The absorbance with wavelength λ of PVA and PVA/MnO$_2$.*
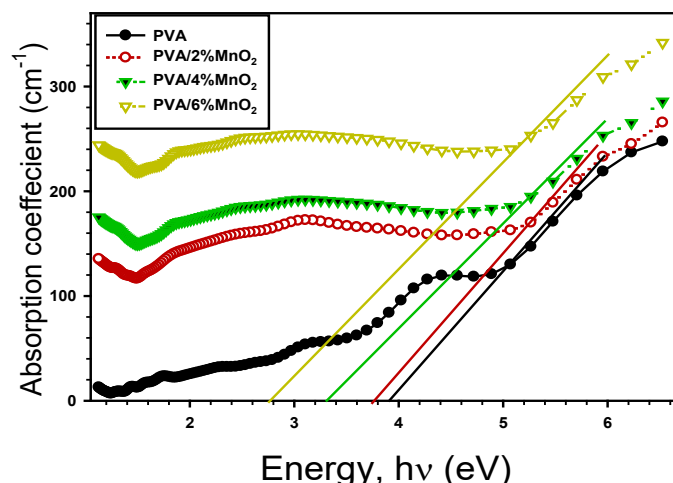
Fig. 11 *The absorbance coefficient with photon energy of PVA and PVA/MnO₂.*

The E_g of PVA and PVA/MnO$_2$ are estimated using Tauc's formula [49]:

$$\alpha h\nu = A \, (h\nu - E_g)^n \tag{9}$$

where, $h\nu = 1240/$, A is Tauc constant, and n is transition type. For transitions between directly forbidden states, directly allowed states, indirectly forbidden states, and indirectly allowed states, n = 3/2, 1/2, 3, and 2 respectively [50]. Figure 12 shows the result of $(\alpha h\nu)^2$ versus $(h\nu)$ to estimate the bandgap of PVA and PVA/MnO$_2$. Table 2 shows that when PVA is combined with amounts of MnO$_2$, the band gap decreases from 5.01 eV for PVA respectively to 4.85, 4.71 and 4.59 eV for PVA/0.02MnO$_2$, PVA/0.04MnO$_2$ and PVA/0.06MnO. The adding of MnO$_2$ particles to PVA causes flaws and link breakage, which contributes to the observed decrease in E_g.

Table 2. E_e, E_g, E_U, and N of PVA and PVA/MnO₂.

	Absorption edge (E_e)	Bandgap (E_g)	Urbach tail(E_U)	Carbon cluster(N)
PVA	3.93	5.01	1.72	48
PVA/0.02MnO$_2$	3.75	4.85	3.12	50
PVA/0.04MnO$_2$	3.31	4.71	3.45	53
PVA/0.06MnO$_2$	2.76	4.59	3.66	56
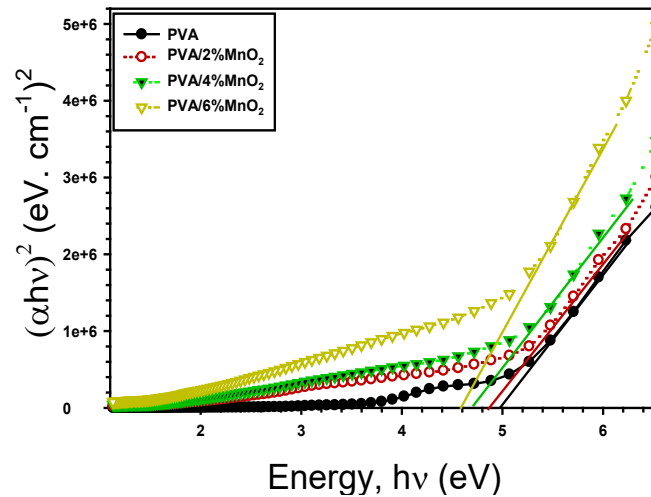
Fig. 12. *The band gap energy with photon energy of PVA and PVA/MnO₂.*

The Urbach tail E_e, which is defined as broad locally concentrated tail is given by [51]:

$$\alpha(\nu) = \alpha_o \; e^{h\nu/E_U} \tag{10}$$

The E_e of PVA and PVA/MnO₂ is given of plot ln (α) with $h\nu$ as indicated in Figure 13. As seen in Table 2, the E_e value of PVA is 1.72 eV and modified to 3.12, 3.45, and 3.66 eV respectively for PVA/0.02MnO₂, PVA/0.04MnO₂ and PVA/0.06MnO₂. The carbonaceous clusters, which are generally related to the bandgap and cluster size is given by [52].

$$E_g = \frac{34.4}{\sqrt{N}} \tag{11}$$

Table 2 records the carbon atoms number (N) is 48 for PVA increased respectively to 50, 53, 56 for PVA/0.02MnO₂, PVA/0.04MnO₂, and PVA/0.06MnO₂. As the MnO₂ content rises, more activities are carried out by the charge carriers, leading to larger clusters and more carbon atoms.
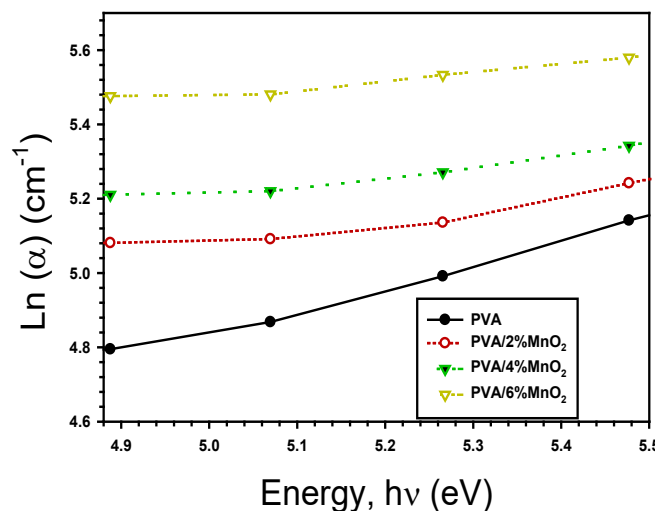
Fig. 13. ln (α) with $h\nu$ of PVA and PVA/MnO₂.

4. Conclusion

XRD and SEM results show that PVA/MnO$_2$ composite films were successfully produced in this study. The results demonstrate that MnO$_2$ interact well with the PVA chains. Furthermore, the optical and dielectric characteristics were determined. At 10^5 Hz, the energy density of PVA is $2.87*10^{-10}$ J/m^3, that rises to $3.34*10^{-10}$ J/m^3 for PVA/2%MnO$_2$ and $4.23*10^{-10}$ J/m^3 for PVA/6%MnO$_2$. This is due to the fact that MnO$_2$ decreasing the needed time for orienting of dipole. Meanwhile, the absorption coefficient and optical band gap of PVA and PVA/MnO$_2$ are calculated. The Urbach energy E_e value of PVA is 1.72 eV and modified to 3.12, 3.45, and 3.66 eV respectively for PVA/0.02MnO$_2$, PVA/0.04MnO$_2$ and PVA/0.06MnO$_2$. The addition of MnO$_2$ causes defects, which made shift in band gap. The results revealed that by incorporating MnO$_2$ into PVA, the optical and dielectric characteristics are enhanced, which could lead to the usage of flexible PVA/MnO$_2$ composite in a wide spectrum of potential devices.

Acknowledgments

References

[1] Zwawi, M., Attar, A., Al-Hossainy, A. F., Abdel-Aziz, M. H., Zoromba, M. S. (2021), Chemical Papers, 75(12), 6575-6589; https://doi.org/10.1007/s11696-021-01830-5

[2] Chaturvedi, A. K., Pappu, A., Srivastava, A. K., & Gupta, M. K. (2021), Materials Letters, 301, 130323; https://doi.org/10.1016/j.matlet.2021.130323

[3] Abutalib, M. M., & Rajeh, A. (2020), Polymer Testing, 91, 106803; https://doi.org/10.1016/j.polymertesting.2020.106803

[4] Li, D., Liu, Y., Shi, S., Li, Y., Geng, C., Xu, S. (2021), Journal of Materials Chemistry C, 9(8), 2873-2881; https://doi.org/10.1039/D0TC05425A

[5] Chaudhuri, B., Ghosh, S., Mondal, B., & Bhadra, D. (2022), Materials Science and Engineering: B, 275, 115500; https://doi.org/10.1016/j.mseb.2021.115500

[6] Altunkaynak, F., Okur, M., & Saracoglu, N. (2022), Journal of Drug Delivery Science and Technology, 68, 103099; https://doi.org/10.1016/j.jddst.2022.103099

[7] Prakash, T., Kumar, E. R., Neri, G., Bawazeer, T. M., Alkhamis, K., Munshi, A., El-Metwaly, N. M. (2022), Ceramics International, 48(1), 1223-1229; https://doi.org/10.1016/j.ceramint.2021.09.207

[8] Dawadi, S., Gupta, A., Khatri, M., Budhathoki, B., Lamichhane, G., Parajuli, N. (2020), Bulletin of Materials 43(1), 1-10; https://doi.org/10.1007/s12034-020-02247-8

[9] Hill, L. I., Portal, R., Verbaere, A., Guyomard, D. (2001), Electrochemical and Solid-State Letters, 4(11), A180; https://doi.org/10.1149/1.1402495

[10] Wang, W., Kan, Y., Yu, B., Pan, Y., Liew, K. M., Song, L., Hu, Y. (2017), Composites Part A: Applied Science and Manufacturing, 95, 173-182; https://doi.org/10.1016/j.compositesa.2017.01.009

[11] Zargar, R. A. (2022), Scientific Reports, 12(1), 1-10; https://doi.org/10.1038/s41598-022-13767-0

[12] Amakoromo, T. E. (2022), Chemical Science International Journal, 31(4), 21-26; https://doi.org/10.9734/CSJI/2022/v31i4816

[13] Algidsawi, A. J. K., Hashim, A., Hadi, A., Habeeb, M. A., Abed, H. H. (2022), Physics and Chemistry of Solid State, 23(2), 353-360; https://doi.org/10.15330/pcss.23.2.353-360

[14] Pashameah, R. A., El-Sharnouby, M., El-Askary, A., El-Morsy, M. A., Ahmed, H. A.,

1062

Menazea, A. A. (2022), Journal of Inorganic and Organometallic Polymers and Materials, 1-10; https://doi.org/10.1007/s10904-022-02311-2

[15] Mohammed, M. I., Khafagy, R. M., Hussien, M. S., Sakr, G. B., Ibrahim, M. A., Yahia, I. S., Zahran, H. Y. (2022), Journal of Materials Science: Materials in Electronics, 33(4), 1977-2002; https://doi.org/10.1007/s10854-021-07402-3

[16] Abdelhamied, M. M., Abdelreheem, A. M., Atta, A. (2022), Plastics, Rubber and Composites, 51(1), 1-12; https://doi.org/10.1080/14658011.2021.1928998

[17] Mohammed, M. I., Yahia, I. S., El-Mongy, S. A. (2022), Optical and Quantum Electronics, 54(9), 1-23; https://doi.org/10.1007/s11082-022-03981-5

[18] Atta, A., Abdelhamied, M. M., Abdelreheem, A. M., Althubiti, N. A. (2022), Inorganic Chemistry Communications, 135, 109085; https://doi.org/10.1016/j.inoche.2021.109085

[19] Abdelhamied, M. M., Atta, A., Abdelreheem, A. M., Farag, A. T. M., El Sherbiny, M. A. (2021), Inorganic Chemistry Communications, 133, 108926; https://doi.org/10.1016/j.inoche.2021.108926

[20] Atta, M. R., Alsulami, Q. A., Asnag, G. M., & Rajeh, A. (2021), Journal of Materials Science: Materials in Electronics, 32(8), 10443-10457; https://doi.org/10.1007/s10854-021-05701-3

[21] Atta, A., Abdel Reheem, A. M., Abdeltwab, E. (2020), Surface Review and Letters, 27(09), 1950214; https://doi.org/10.1142/S0218625X19502147

[22] Pashameah, R. A., El-Sharnouby, M., El-Askary, A., El-Morsy, M. A., Ahmed, H. A., Menazea, A. A. (2022), Journal of Inorganic and Organometallic Polymers and Materials, 1-10; https://doi.org/10.1007/s10904-022-02311-2

[23] Abdeltwab, E., Atta, A. (2021), Surface Innovations, 40, 1-9.

[24] El-Dafrawy, S. M., Tarek, M., Samra, S., Hassan, S. M. (2021), Scientific Reports, 11(1), 1-11; https://doi.org/10.1038/s41598-021-90846-8

[25] Abdeltwab, E., & Atta, A. (2021), International Journal of Modern Physics B, 35(30), 2150310; https://doi.org/10.1142/S0217979221503100

[26] Majeed, A. H., Al-Tikrity, E. T. B., Hussain, D. H. (2021), Polymers and Polymer Composites, 29(7), 1089-1100; https://doi.org/10.1177/0967391120951406

[27] Ishaq, S., Kanwal, F., Atiq, S., Moussa, M., Azhar, U., Gul, I., Losic, D. (2018). Results in Physics, 11, 540-548; https://doi.org/10.1016/j.rinp.2018.09.049

[28] Atta, A. (2020), Surface Innovations, 9(1), 17-24; https://doi.org/10.1680/jsuin.20.00020

[29] Atta, A., Lotfy, S., & Abdeltwab, E. (2018), Journal of Applied Polymer Science, 135(33), 46647; https://doi.org/10.1002/app.46647

[30] Singla, M.; Sehrawat, R.; Rana, N.; Singh, K., Journal of Nanoparticle Research 2011, 13 (5), 2109-2116; https://doi.org/10.1007/s11051-010-9968-4

[31] Zhang, Y.; Wang, Y.; Deng, Y.; Li, M.; Bai, J., ACS applied materials & interfaces 2012, 4 (1), 65-68; https://doi.org/10.1021/am2016156

[32] Kumar, M.; Srivastava, N., Journal of Non-Crystalline Solids 2014, 389, 28-34; https://doi.org/10.1016/j.jnoncrysol.2014.02.002

[33] Wang, G.-S.; Wu, Y.-Y.; Zhang, X.-J.; Li, Y.; Guo, L.; Cao, M.-S., Journal of Materials Chemistry A 2014, 2 (23), 8644-8651; https://doi.org/10.1039/C4TA00485J

[34] I. Latif, E.E. AL-Abodi, D.H. Badri, J. Al Khafagi, American Journal of Polymer Science 2 (2012) 135-140; https://doi.org/10.5923/j.ajps.20120206.01

[35] R. Thangarasu, N. Senthilkumar, B. Babu, K. Mohanraj, J. Chandrasekaran, O. Balasundaram, Journal of Advanced Physics 7 (2018) 312-318; https://doi.org/10.1166/jap.2018.1442

[36] Wu, W., Huang, X., Li, S., Jiang, P., & Toshikatsu, T. (2012), The Journal of Physical Chemistry C, 116(47), 24887-24895; https://doi.org/10.1021/jp3088644

[37] Hemalatha, K. S., Sriprakash, G., Ambika Prasad, M. V. N., Damle, R., Rukmani, K. (2015), Journal of Applied physics, 118(15), 154103; https://doi.org/10.1063/1.4933286

[38] Choudhary, S. (2017), Physica B: Condensed Matter, 522, 48-56;

https://doi.org/10.1016/j.physb.2017.07.066

[39] R. Gupta, R. Kumar, Nano-Structures & Nano-Objects 18 (2019) 100318;
https://doi.org/10.1016/j.nanoso.2019.100318

[40] G. Sahu, M. Das, M. Yadav, B.P. Sahoo, J. Tripathy, Polymers 12 (2020) 374;
https://doi.org/10.3390/polym12020374

[41] S. Atiq, M. Majeed, A. Ahmad, S.K. Abbas, M. Saleem, S. Riaz, S. Naseem, Ceramics International 43 (2017) 2486-2494; https://doi.org/10.1016/j.ceramint.2016.11.046

[42] W. Jilani, N. Fourati, C. Zerrouki, O. Gallot-Lavallée, H. Guermazi, Journal of Inorganic and Organometallic Polymers and Materials 29 (2019) 456-464; https://doi.org/10.1007/s10904-018-1016-3

[43] Bouaamlat, H., Hadi, N., Belghiti, N., Sadki, H., Naciri Bennani, M., Abdi, F. Abarkan, M. (2020), Advances in Materials Science and Engineering, 2020;
https://doi.org/10.1155/2020/8689150

[44] A. Hashim, A. Hadi, Ukrainian Journal of Physics 63 (2018) 754-754;
https://doi.org/10.15407/ujpe63.8.754

[45] H. Ahmed, A. Hashim, Egyptian Journal of Chemistry 63 (2020) 805-811.

[46] Prabakaran, S., Nisha, K. D., Harish, S., Archana, J., Navaneethan, M. (2021), Journal of Alloys and Compounds, 885, 160936; https://doi.org/10.1016/j.jallcom.2021.160936

[47] Abdel Reheem, A.; Atta, A.; Afify, T., Surface Review &Letters 2017, 24 (03), 1750038;
https://doi.org/10.1142/S0218625X1750038X

[48] Abdelhamied, M. M., Atta, A., Abdelreheem, A. M., Farag, A. T. M., El Okr, M. M. (2020), Journal of Materials Science: Materials in Electronics, 31(24), 22629-22641;
https://doi.org/10.1007/s10854-020-04774-w

[49] Naik, R., Ganesan, R., & Sangunni, K. S. (2013), Journal of alloys and compounds, 554, 293-298; https://doi.org/10.1016/j.jallcom.2012.11.198

[50] Naik, R., Ganesan, R., & Sangunni, K. S. (2010), Journal of alloys and compounds, 505(1), 249-254; https://doi.org/10.1016/j.jallcom.2010.06.039

[51] Taha T, Hendawy N, El-Rabaie S, Esmat A and El-Mansy M (2019), Polymer Bulletin, 76: 4769-4784; https://doi.org/10.1007/s00289-018-2633-2

[52] Atta, A., Alotaibi, B. M., Abdelhamied, M. M. (2022), Inorganic Chemistry Communications, 141, 109502; https://doi.org/10.1016/j.inoche.2022.109502